OPEN

Citation: Cell Death and Disease (2013) 4, e651; doi:10.1038/cddis.2013.177

www.nature.com/cddis

Protogenin prevents premature apoptosis of rostral cephalic neural crest cells by activating the $\alpha5\beta1$-integrin

Y-C Wang[1], H-C Juan[2], Y-H Wong[1], W-C Kuo[2], Y-L Lu[1], S-F Lin[3], C-J Lu[1] and M-J Fann*[,2,4]

The bones and connective tissues of the murine jaws and skull are partly derived from cephalic neural crest cells (CNCCs). Here, we report that mice deficient of protogenin (Prtg) protein, an immunoglobulin domain-containing receptor expressed in the developing nervous system, have impairments of the palatine and skull. Data from lineage tracing experiments, expression patterns of neural crest cell (NCC) marker genes and detection of apoptotic cells indicate that the malformation of bones in *Prtg*-deficient mice is due to increased apoptosis of rostral CNCCs (R-CNCCs). Using a yeast two-hybrid screening, we found that Prtg interacts with Radil, a protein previously shown to affect the migration and survival of NCCs in zebrafish with unknown mechanism. Overexpression of Prtg induces translocation of Radil from cytoplasm to cell membrane in cultured AD293 cells. In addition, overexpression of Prtg and Radil activates $\alpha5\beta1$-integrins to high-affinity conformational forms, which is further enhanced by the addition of Prtg ligand ERdj3 into cultured cells. Blockage of Radil by RNA interference abolishes the effect of ERdj3 and Prtg on the $\alpha5\beta1$-integrin, suggesting that Radil acts downstream of Prtg. *Prtg*-deficient R-CNCCs display fewer activated $\alpha5\beta1$-integrins in embryos, and these cells show reduced migratory ability in *in vitro* transwell assay. These results suggest that the inside-out activation of the $\alpha5\beta1$-integrin mediated by ERdj3/Prtg/Radil signaling is crucial for proper functions of R-CNCCs, and the deficiency of this pathway causes premature apoptosis of a subset of R-CNCCs and malformation of craniofacial structures.

Cell Death and Disease (2013) **4,** e651; doi:10.1038/cddis.2013.177; published online 6 June 2013
Subject Category: Neuroscience

Congenital craniofacial defects are the most common birth defects in human. Many craniofacial syndromes, such as the Collins, Robin and Di George syndromes, are associated with defects in neural crest (NC) development.[1] In rodents, jaws and the skull vault are derived from the cephalic NC cells (CNCCs) and the head paraxial mesoderm cells.[2] In the mouse embryo, the rostral CNCCs (R-CNCCs) originate from NC between diencephalon to rhombomere 2 (r2) and undergo an epithelial–mesenchymal transition at embryonic day 8.5 (E8.5), colonize the frontonasal primordium and branchial arch 1 (BA1) at E9–9.5 and later give rise to the skull, the frontonasal skeleton and anterior part of the lower jaw.[3,4] Originated from NC between r4 and r8, caudal CNCCs (C-CNCCs) enter into BA2–6 and form connective tissues, smooth muscle cells and the pericytes of the blood vessels within the neck and cardiovascular structures.[5,6,7] Notably, trunk NC cells (TNCCs) do not form skeletal tissues. In addition to CNCCs, a part of posterior skull vault and the majority of skeletons in posterior upper jaw are contributed by derivatives of head paraxial mesoderm.[8]

It has been shown that integrins are critical molecules for proper development of NC cells (NCCs), and perturbation of integrin molecules may lead to immobility and apoptosis of NCCs. Bronner–Fraser showed that neutralization of antibodies against the $\beta1$-integrin reduces R-CNCC migration in chick embryos.[9,10] Blockage of multiple integrins containing $\beta1$ and $\alpha3$ subunits inhibits migration of cultured avian TNCCs.[11] Similarly, expression of the $\alpha5\beta1$-integrin is required for *Xenopus* CNCC migration on fibronectin[12] and there is an increase of cell death of migrating CNCCs in the $\alpha5$-integrin-deficient mice.[13] In addition, conformational changes of the extracellular domain of integrin heterodimers is another regulatory step for integrin effects on NCC development.[14] However, how integrin conformation in NCCs is modulated remains unknown.

Many immunoglobulin family members are expressed in the developing nervous system with undefined functions. Here, we explore functions of one immunoglobulin family member, namely protogenin (Prtg) protein. Prtg protein is restrictedly expressed between E7 and E10 in mouse embryo and acts as

[1]Institute of Neuroscience, National Yang-Ming University, Taipei, Taiwan 112, Republic of China; [2]Department of Life Sciences and Institute of Genome Sciences, National Yang-Ming University, Taipei, Taiwan 112, Republic of China; [3]Instrumentation Resource Center, National Yang-Ming University, Taipei, Taiwan 112, Republic of China and [4]Brain Research Center, National Yang-Ming University, Taipei, Taiwan 112, Republic of China
*Corresponding author: M-J Fann, Department of Life Sciences and Institute of Genome Sciences, National Yang-Ming University, No.155, Sec. 2, Linong Street, Taipei, Taiwan 112, Republic of China. Tel: +886 2 2826 7184; Fax: +886 2 2823 4898; E-mail: mjfann@ym.edu.tw
Keywords: Radil; branchial arches; bone formation; integrin
Abbreviation: BA, branchial arch; CM, conditioned medium; CNCCs, cephalic neural crest cells; C-CNCCs, caudal cephalic neural crest cells; E8.5, embryonic day 8.5; NC, neural crest; NCCs, neural crest cells; non-TNCCs, trunk non-neural crest cells; Prtg, protogenin; Prtg-f, full-length Prtg; Prtg-c, Prtg cytoplasmic domain; PrtgΔc, cytosolic domain-deleted Prtg; r2, rhombomere 2; RC, rostral cephalic; R-CNCCs, rostral cephalic neural crest cells; R-non-CNCCs, rostral non-cephlaic neural crest cells; TNCCs, trunk neural crest cells; TUNEL, terminal deoxynucleotidyl transferase dUTP nick-end labeling
Received 07.12.12; revised 26.3.13; accepted 29.4.13; Edited by A Verkhratsky

a receptor by binding its ligand ERdj3.[15] Although many activities of Prtg have been demonstrated *in vitro* and in chick embryos,[15–17] roles of Prtg during mouse development are still unclear. In this study, we generated conventional *Prtg* knockout mutant mice. Defects of the craniofacial structure are observed in the neonatal *Prtg* mutants. We demonstrate that the defective skeletal phenotypes are due to abnormal apoptosis of R-CNCCs at E9–E10. The participating molecules involved in Prtg signaling include Radil and high-affinity conformational forms of the $\alpha5\beta1$-integrin.

Results

Generation of *Prtg* knockout mice. A targeting vector that replaces exons 3–7 of the *Prtg* gene with the *IRES-lacZ* gene upon homologous recombination was generated (Figure 1a). Insertion of *IRES-lacZ* into the *Prtg* genome creates a premature termination of the Prtg protein and results in a peptide containing only the first 137 amino acids out of total 1192 amino acids. Germline transmission of the targeted allele was verified by Southern blotting (Figure 1b). No full-length Prtg (Prtg-f) protein is expressed in homozygous mice and about half of the amount of Prtg protein is present in heterozygous mice (Figure 1c). Results from immunofluoresence staining confirm that no Prtg protein is expressed in homozygous mice (Figure 1d).

***Prtg*$^{-/-}$ mice have abnormality of craniofacial skeletons and cartilages.** Heterozygous *Prtg*$^{+/-}$ mice are morphologically normal and fertile. The mating between heterozygous *Prtg*$^{+/-}$ mice produces *Prtg*$^{-/-}$ homozygous neonates that are born with a normal Mendelian ratio, but have a higher mortality. In all, 44.4% of neonatal *Prtg*$^{-/-}$ homozygous mice die within 72 h of birth. Another 11.1% of *Prtg*$^{-/-}$ mice exhibit growth retardation and die before postnatal day 14; this is apparently due to malnutrition, which is revealed by smaller body sizes and delayed body-weight gain (data not shown). The remaining *Prtg*$^{-/-}$ mutants survive to adulthood and are fertile. The progeny from mating between homozygous mice still exhibits the $\sim$45% mortality rate within the first 3 days. We thus focused on finding the defects that are responsible for the death of the *Prtg*$^{-/-}$ mutants within 72 h after birth.

As neonatal homozygotes have lower amounts or no milk in their stomachs (Figure 1f), we examined the enteric nervous system by measuring acetylcholinesterase activity in P1 gastrointestinal tract. There is no apparent difference of neuronal innervation in the intestine between the wild-type and *Prtg*$^{-/-}$ mice (Figures 1g and h). Examination of the developing nervous system in E10.5 embryos by whole-mount staining using antibody against 165-kDa neurofilament reveals no abnormalities in the *Prtg*$^{-/-}$ embryos (Figure 1j). The gross morphology of the cerebral cortex, hippocampus, eye, olfactory bulb, cerebellum and spinal cord in P1 *Prtg*$^{-/-}$ mutants is normal by eosin and hematoxylin staining (data not shown).

Defective nasal structures including the palatal bones and/or nasal septum may bring about ingestion difficulty and/or a respiration deficiency, causing the death of the neonatal *Prtg*$^{-/-}$ pups. Thus, we examined the cranial bones and cartilage of the P1 *Prtg*$^{-/-}$ mutants with Alizarin red and Alcian blue staining. The *Prtg*$^{-/-}$ mutants are found to have a shorter and thinner nasal septum (black-dotted circle in Figure 1l). In some severe cases, there is no nasal septum. Incomplete fusion of the basisphenoid bone is also observed in the *Prtg* knockout mice (arrow in Figure 1l). In addition, the palatine of the *Prtg*$^{-/-}$ mice is found to be thinner (arrow in Figure 1m). Furthermore, the *Prtg*$^{-/-}$ mutants displayed a loss of branches of the ala temporalis and less mineralization of the parietal bone, temporal bone and supraoccipital bone (Figures 1p and r). The penetrance of skeletal defects ranges from 42.8 to 61.1% (Figure 1s). It is noted that all survived mutant pups contain normal nasal septum and palatine when examined at P4, suggesting that the cause of perinatal death is likely due to defects of these two structures.

Fewer rostral CNCCs are present in the *Prtg*$^{-/-}$ mouse embryos. The observed craniofacial defects of *Prtg*$^{-/-}$ mutants are in structures that are developmentally derived from R-CNCCs and head paraxial mesoderm (Figure 1s). We conducted lineage tracing experiments by generating *Prtg*$^{-/-}$ mutants with a *Wnt1-Cre;R26R* genetic background in which the NC-derived cells are marked with β-galactosidase.[18,19] When *Prtg*$^{-/-}$*;Wnt1-Cre;R26R* embryos were examined at E10.5, fewer X-gal^{+} cells were detected in the diencephalon, mesencephalon and frontonasal primordium compared wih those in the heterozygous embryos (arrowheads in Figures 2a and b, $n=6$ for each genome type). In addition, there are also fewer X-gal^{+} cells in dorsal midbrain, frontonasal process and upper jaw region

Figure 1 Abnormalities of the craniofacial bones in *Prtg*$^{-/-}$ mice. (**a**) Schematic diagrams depicting the targeting vector, *Prtg* locus and the predicted recombinant allele. (**b**) Germline transmission of the targeted allele was verified by Southern blotting. The expected sizes of the DNA fragments are marked (arrowheads). WT: wild type; Mut: mutant. (**c**) Tissue extracts of E9.5 wild-type, *Prtg*$^{+/-}$ and *Prtg*$^{-/-}$ embryos were subjected to western blot analysis using anti-Prtg antibody. (**d**) Results from immunofluorescence staining of Prtg protein (red) in transverse sections of E9.5 *Prtg*$^{-/-}$ embryos demonstrate no expression of Prtg protein in *Prtg*$^{-/-}$ embryos. Nuclei are labeled with DAPI (blue). (**e**) Appearance of the P1 wild-type mouse. (**f**) The P1 *Prtg*$^{-/-}$ mouse has the same body size as the wild-type mouse, but has less milk in the stomach (arrow and lower right panel). (**g**, **h**) Histochemical staining of acetylcholinesterase activity in the duodenum of P1 *Prtg*$^{+/+}$ (**g**) and *Prtg*$^{-/-}$ (**h**) neonates was examined ($n=11$). (**i**, **j**) Whole-mount neurofilament staining was performed on E10.5 *Prtg*$^{+/+}$ (**i**) and *Prtg*$^{-/-}$ (**j**) embryos. No abnormalities of cranial and spinal nerves were detected in *Prtg*$^{-/-}$ embryos ($n=9$). (**k–r**) The morphology of the craniofacial skeletal structures and skull vault of P1 wild-type (**k**, **m**, **o**, **q**) and *Prtg*$^{-/-}$ (**l**, **n**, **p**, **r**) mice as revealed by Alcian blue and/or Alizarin red staining. (**k**, **l**) Dorsal views of the palatal bones after the skull is removed show the disappearance of the nasal septum (black dotted outline) and an aperture in basisphenoid bone (arrow) in the *Prtg*$^{-/-}$ mice. (**m**, **n**) Coronal sections of the palatine display a thinner palatal bone (arrow) in the *Prtg*$^{-/-}$ mice. (**o**, **p**) Branches (arrow) of ala temporalis (black dotted outline) become shorter or disappear in *Prtg*$^{-/-}$ mice. (**q**, **r**) Lateral views of the skull vault show that mineralization of the parietal bone (yellow dotted outline) and the supraoccipital bone (red dotted outline) is incomplete in the *Prtg*$^{-/-}$ mice. (**s**) A schematic presentation of the craniofacial defects in *Prtg*$^{-/-}$ mice is shown in the left. Defective bones (red) and cartilages (blue) are marked. Cell lineage and penetrance of the craniofacial defects observed in *Prtg*$^{-/-}$ mice, and numbers of mice analyzed are indicated in the right

of the E13.5 homozygous embryos (Figures 2c and d, $n=7$ for each genome type). These results suggest that fewer R-CNCCs are present in *Prtg*$^{-/-}$ mutants. Notably, there is no defect in the X-gal-staining patterns of the dorsal root ganglia that develop from TNCCs in homozygous embryos.

To confirm that there are losses of R-CNCCs in the absence of Prtg protein, we analyzed expression patterns in E9–E10 embryos of several NCC markers, which are also critical for the development of craniofacial structures by whole-mount *in situ* hybridization. In wild-type embryos, the expression of

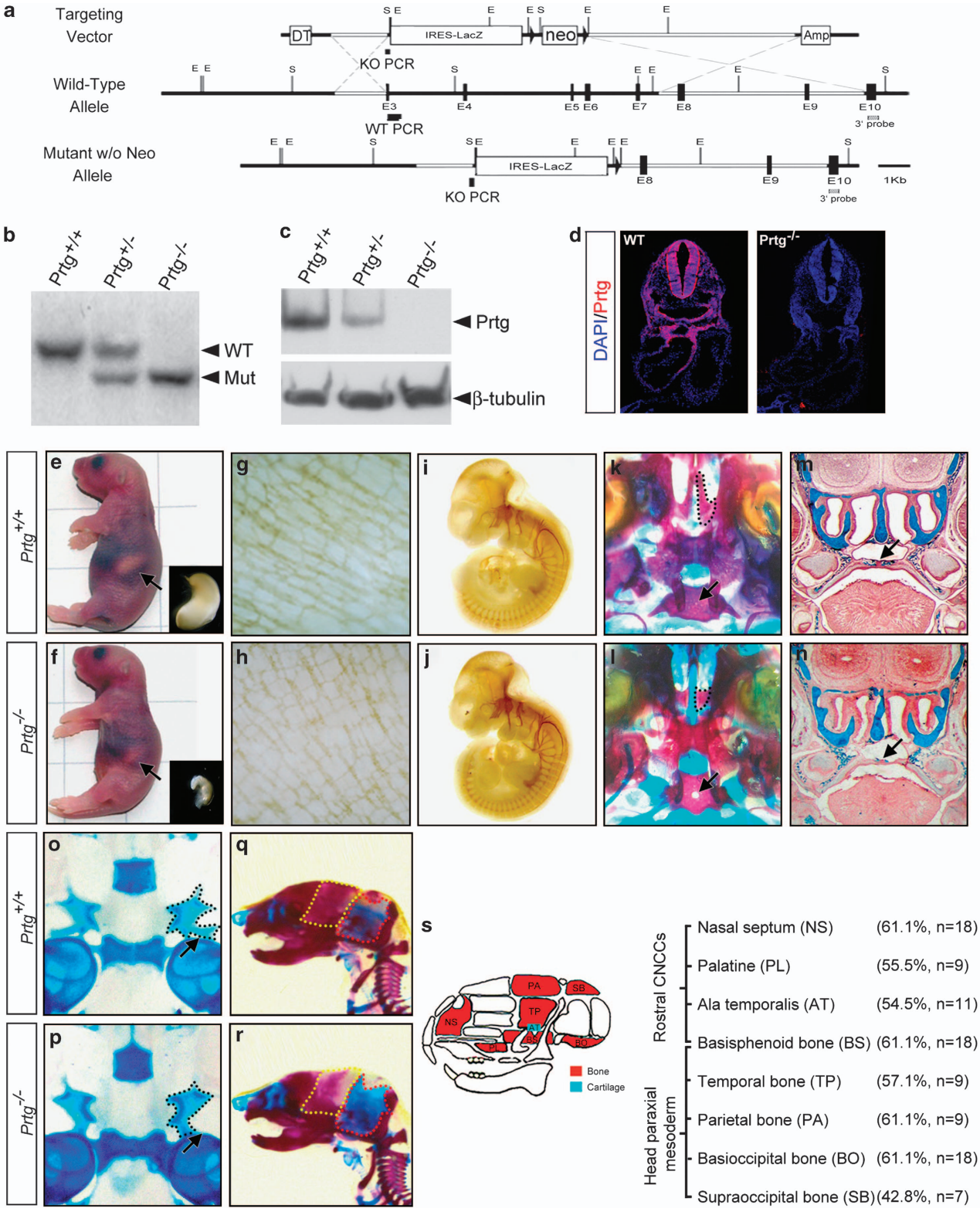

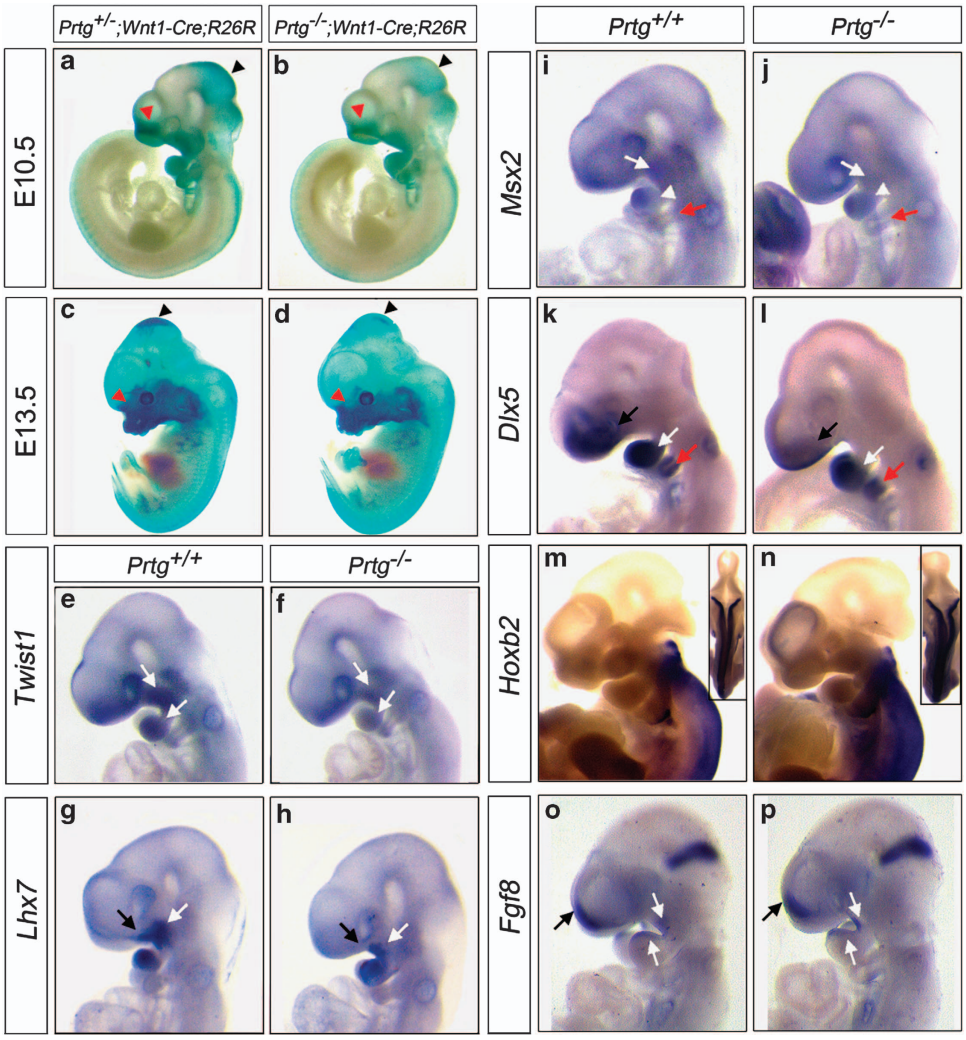

Figure 2 Loss of R-CNCCs in *Prtg*$^{-/-}$ embryos. (**a**–**d**) Embryos of *Prtg*$^{+/-}$;*Wnt1-Cre;R26R* and *Prtg*$^{-/-}$;*Wnt1-Cre;R26R* were subjected to X-gal lineage tracing analysis. (**a**, **b**) E10.5 ($n=6$); (**c**, **d**) E13.5 ($n=7$). Fewer R-CNCCs are detected in dorsal midbrain (black arrowhead) and frontonasal primordium (red arrowhead) of *Prtg*$^{-/-}$;*Wnt1-Cre;R26R* embryos than in heterozygous embryos. (**e**–**n**) *In situ* hybridization of the indicated genes was performed in E9.5 wild-type and *Prtg*$^{-/-}$ embryos. (**e**, **f**) Expression of *Twist1* in the maxilla and mandible of BA1 (white arrows) is reduced in *Prtg*$^{-/-}$ mice ($n=8$ for both genome types). (**g**–**h**) Expression of *Lhx7* is reduced in the frontonasal primordium (black arrows) and maxilla (white arrows) in *Prtg*$^{-/-}$ mice ($n=8$). (**i**, **j**) In *Prtg*$^{-/-}$ mice, expression of *Msx2* in the maxilla disappears (white arrows). Weaker expression of *Msx2* is detected in the mandible (white arrowheads) and there is no change in the BA2 and BA3 (red arrows) ($n=9$). (**k**, **l**) *Dlx5* is slightly reduced in the frontonasal primordium (black arrows) and mandible (white arrows). No difference of *Dlx5* expression in the BA2 and BA3 (red arrows) between the wild-type and *Prtg*$^{-/-}$ embryos is detected ($n=8$). (**m**, **n**) Expression of *Hoxb2* in E10 embryos was analyzed. Insets are dorsal views of the embryos ($n=4$). (**o**, **p**) Expression of *Fgf8* in E9.5 embryos was analyzed. Expression of *Fgf8* in the anterior neural ridge (black arrows) and BA1 epithelium (white arrows) is the same between wild-type and mutant embryos ($n=8$)

Twist1 is detected in the maxilla and mandible of BA1. A drastic decrease in *Twist1* expression in BA1 is detected in *Prtg*$^{-/-}$ mutants (Figure 2f). Diminished *Lhx7* in the frontonasal process and the maxilla of BA1 is also observed in *Prtg*$^{-/-}$ mutants (arrows in Figure 2h). To examine whether C-CNCCs are defective in *Prtg*$^{-/-}$ mutant embryos, we analyzed expression of *Msx2*, a marker for NCCs derived from posterior midbrain to rhombencephalon NC.[20] Although a decrease in *Msx2* expression is detected in the maxilla and mandible of *Prtg*$^{-/-}$ mutant embryos at E9.5 (white arrows in Figure 2j), expression of *Msx2* in BA2 and BA3 is the same between wild-type and *Prtg*$^{-/-}$ mice (red arrows in Figures 2i and j). Analysis of *Dlx5* expression also indicates that the development of BA2 and BA3 is normal in the *Prtg*$^{-/-}$ mutants (red arrow in Figure 2l). To further validate that the effects of Prtg activity are restricted to R-CNCCs, we analyzed the expression of *Hoxb2*, a known marker that defines the identities of NC for C-CNCCs and TNCCs.[21] The anterior boundary and the level of *Hoxb2* expression in *Prtg*$^{-/-}$ mutant embryos are the same as in wild-type embryos (Figures 2m and n), supporting that loss of Prtg does not affect the development of C-CNCCs and TNCCs. Similarly, loss of Prtg activity does not alter the expression of *Fgf8*, an important growth factor for CNCCs,[22] in anterior neural ridge and BA1 epithelium (arrows in Figures 2o and p).

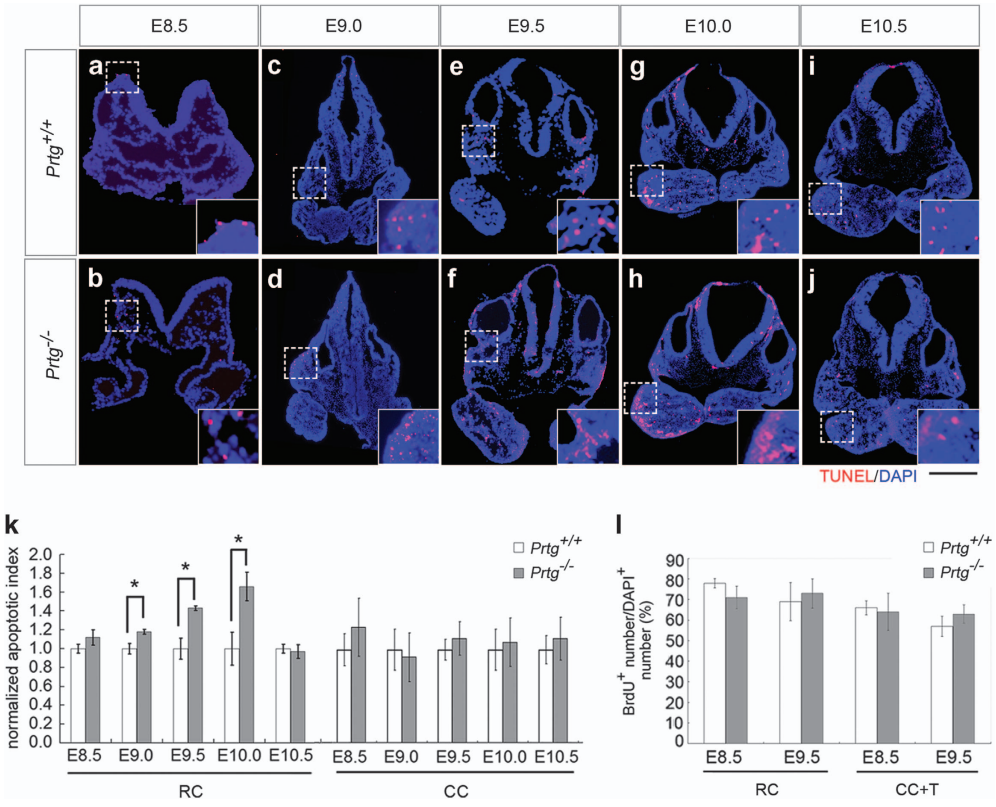

Figure 3 Increased apoptosis in the rostral cephalic region in *Prtg*$^{-/-}$ embryos. Transverse 12-μm sections of *Prtg*$^{+/+}$ (**a**, **c**, **e**, **g**, **i**) and *Prtg*$^{-/-}$ embryos (**b**, **d**, **f**, **h**, **j**) were subjected to TUNEL analysis. (**a**, **b**) E8.5; (**c**, **d**) E9.0; (**e**, **f**) E9.5; (**g**, **h**) E10.0 and (**i**, **j**) E10.5. Higher magnifications of white boxes are shown in lower right corners. Scale bar, 300 μm for (**a**) and (**b**); 500 μm for (**c**–**f**); 600 μm for (**g**, **h**) and 800 μm for (**i**, **j**). (**k**) Quantification of TUNEL-positive cells shown in (**a**)–(**j**). All 12-μm sections from the E8.5 embryos and every other section from the E9.0–E10.5 embryos were subjected to TUNEL assay. Numbers of TUNEL-positive cells were counted and normalized against the DAPI intensities. Data are further normalized against those of *Prtg*$^{+/-}$ embryos and shown as the mean ± S.E.M. ($n=4$; $^*P<0.05$, by Student's *t*-test). RC: rostral cephalic; CC: caudal cephalic. (**l**) Proliferation analysis. *Prtg*$^{+/-}$ and *Prtg*$^{-/-}$ embryos at E8.5 or E9.5 were harvested after 6-h BrdU labeling. Detection of BrdU in RC and CC/trunk (CC + T) regions was performed on 20-μm transverse sections. Five sections of each region were randomly selected and numbers of BrdU$^+$ and DAPI$^+$ cells were counted. The results are shown as the mean ± S.E.M. ($n=4$)

Prtg is involved in the survival but not proliferation of rostral CNCCs. Fewer R-CNCCs present in *Prtg*$^{-/-}$ embryos could be due to cell death and/or decreased cell proliferation. To discriminate these possibilities, we conducted a terminal deoxynucleotidyl transferase dUTP nick end labeling (TUNEL) assay to detect whether there is a change in cell survival in *Prtg*$^{-/-}$ embryos. In the rostral cephalic sections, there are 18 ± 2.6% more TUNEL$^+$ cells in E9.0 *Prtg*$^{-/-}$ embryos, 43 ± 2.2% more TUNEL$^+$ cells in E9.5 *Prtg*$^{-/-}$ embryos and 66 ± 15% more TUNEL$^+$ cells in E10.0 *Prtg*$^{-/-}$ embryos compared with *Prtg*$^{+/-}$ embryos (Figures 3a–k). The increase in TUNEL$^+$ cells is spatially restricted to rostral cephalic region and temporally to the period between E9.0 and E10.0. We also performed a 6-h BrdU labeling for cell proliferation analysis in E8.5 and E9.5 *Prtg*$^{-/-}$ embryos during the time when expression of the Prtg protein is at its highest. There is no decrease of cell proliferation rate in rostral and caudal cephalic/trunk sections at either time points (Figure 3l, and data not shown).

To verify that the increased TUNEL$^+$ cells are NCCs, mouse embryos with a *Wnt1-Cre;CAT-EGFPflox* genetic background are used. Apoptotic cells are revealed by cleaved caspase 3 (cCasp3) staining. Colocalization of cCasp3$^+$ and EGFP$^+$ staining indicates that the apoptotic cells are NCCs. At E9.5, there is a 95 ± 22% more cCasp3$^+$/EGFP$^+$ R-CNCCs in the *Prtg*$^{-/-}$ mutant embryos compared with heterozygous embryos (Figures 4a–h and y). No increase of cell death is observed in TNCCs of *Prtg*$^{-/-}$;*Wnt1-Cre;CAT-EGFPflox* embryos (Figures 4i–l and y). Furthermore, apoptosis among non-NCCs (cCasp3$^+$/EGFP$^-$ cells) along the entire body axis is the same between heterozygous and homozygous embryos (Figure 4y). These results reveal that the increase in apoptotic cells observed in the rostral cephalic region of the *Prtg*$^{-/-}$ embryos during E9–E10, as shown in Figure 3, are likely to involve R-CNCCs. Note that no increase of apoptotic cells are observed in dorsal neural tube (Figure 3b), suggesting that Prtg dose not affect delamination of CNCCs from the neural tube.

As a part of craniofacial skeletal defects exhibited in P1 *Prtg*$^{-/-}$ mutants is derived from the head paraxial mesoderm lineage, we conducted TUNEL experiments using *Mesp1-Cre;CAT-EGFPflox* mice[18] to examine effects of Prtg protein on mesoderm derivatives. It was found that few apoptotic cells are paraxial mesoderm-derived cells in rostral cephalic region (white arrows in Figures 4m–t and z) and trunk region (Figures 4u–x and z) of either E10 *Prtg*$^{+/-}$;

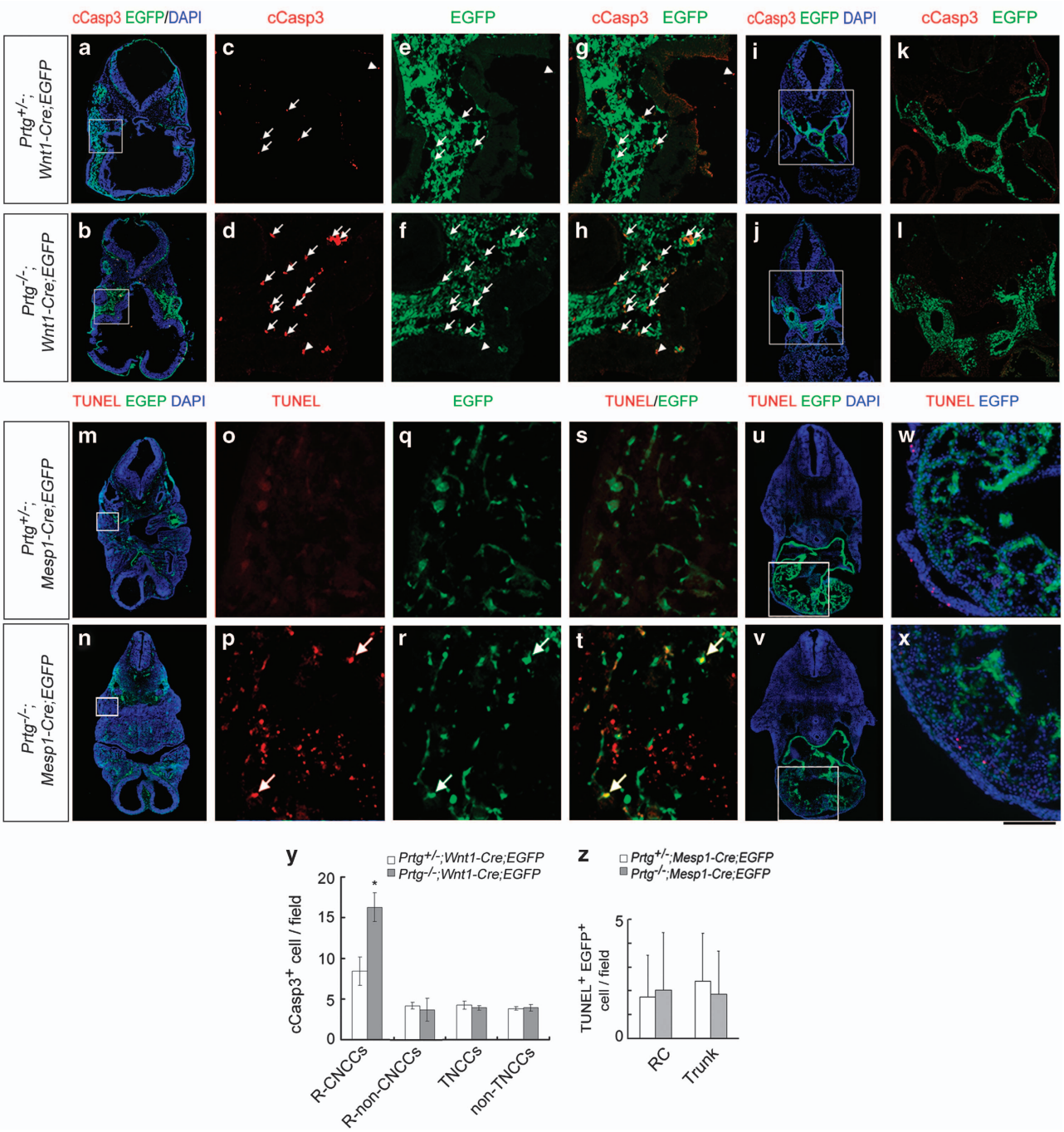

Figure 4 Increase of apoptotic R-CNCCs in E9.5 embryos. (**a**–**l**) Transverse sections of E9.5 *Prtg*$^{+/-}$;*Wnt1-Cre;CAT-EGFPflox* and *Prtg*$^{-/-}$; *Wnt1-Cre; CAT-EGFPflox* embryos were labeled with the antibody against cCasp3. (**a**–**h**) At the rostral cephalic level. cCasp3^{+}/EGFP^{+} cells are marked with white arrows and cCasp3^{+}/EGFP^{-} cells are marked with white arrowheads. (**c**, **e**, **g**) and (**d**, **f**, **h**) are higher magnifications of the white boxes in (**a**) and (**b**). (**i**–**l**) At the trunk level. (**k**) and (**l**) are higher magnifications of the white boxes in (**i**) and (**j**). (**m**–**x**) Transverse sections of E10 *Prtg*$^{+/-}$;*Mesp1-Cre;CAT*-EGFP*flox* and *Prtg*$^{-/-}$;*Mesp1-Cre;CAT-EGFPflox* embryos were subjected to TUNEL assay. (**m**–**t**) At the rostral cephalic level. (**u**–**x**) At the trunk level. White arrows mark TUNEL^{+}/EGFP^{+} cells. (**o**, **q**, **s**) and (**p**, **r**, **t**) are higher magnifications of the white boxes in (**m**) and (**n**). (**w**) and (**x**) are higher magnifications of the white boxes in (**u**) and (**v**). Scale bar, 600 μm for (**a**, **b**), (**i**, **j**, **m**, **n**, **u**, **v**); 125 μm for C–H; 250 μm for (**k**, **l**); 100 μm for (**o**–**t**) and (**w**, **x**). (**y**) Quantification of the apoptotic cells in *Prtg*$^{+/-}$;*Wnt1-Cre;CAT-EGFPflox* and *Prtg*$^{-/-}$; *Wnt1-Cre;CAT-EGFPflox* embryos at levels of rostral cephalic and trunk regions. All sections were examined for EGFP and cCasp3 staining. The numbers of the cCasp3^{+} cells per field were counted. The results are shown as the mean ± S.E.M. ($n=4$; *$P<0.05$, by Student's *t*-test). R-non-CNCCs: rostral non-cephalic NCCs; non-TNCCs: trunk non-NCCs. (**z**) TUNEL^{+}/EGFP^{+} cells in *Prtg*$^{+/-}$;*Mesp1-Cre;CAT*-EGFP*flox* and *Prtg*$^{-/-}$;*Mesp1-Cre;CAT-EGFPflox* embryos were quantified and shown as the mean ± S.E.M. ($n=4$). RC: rostral cephalic level

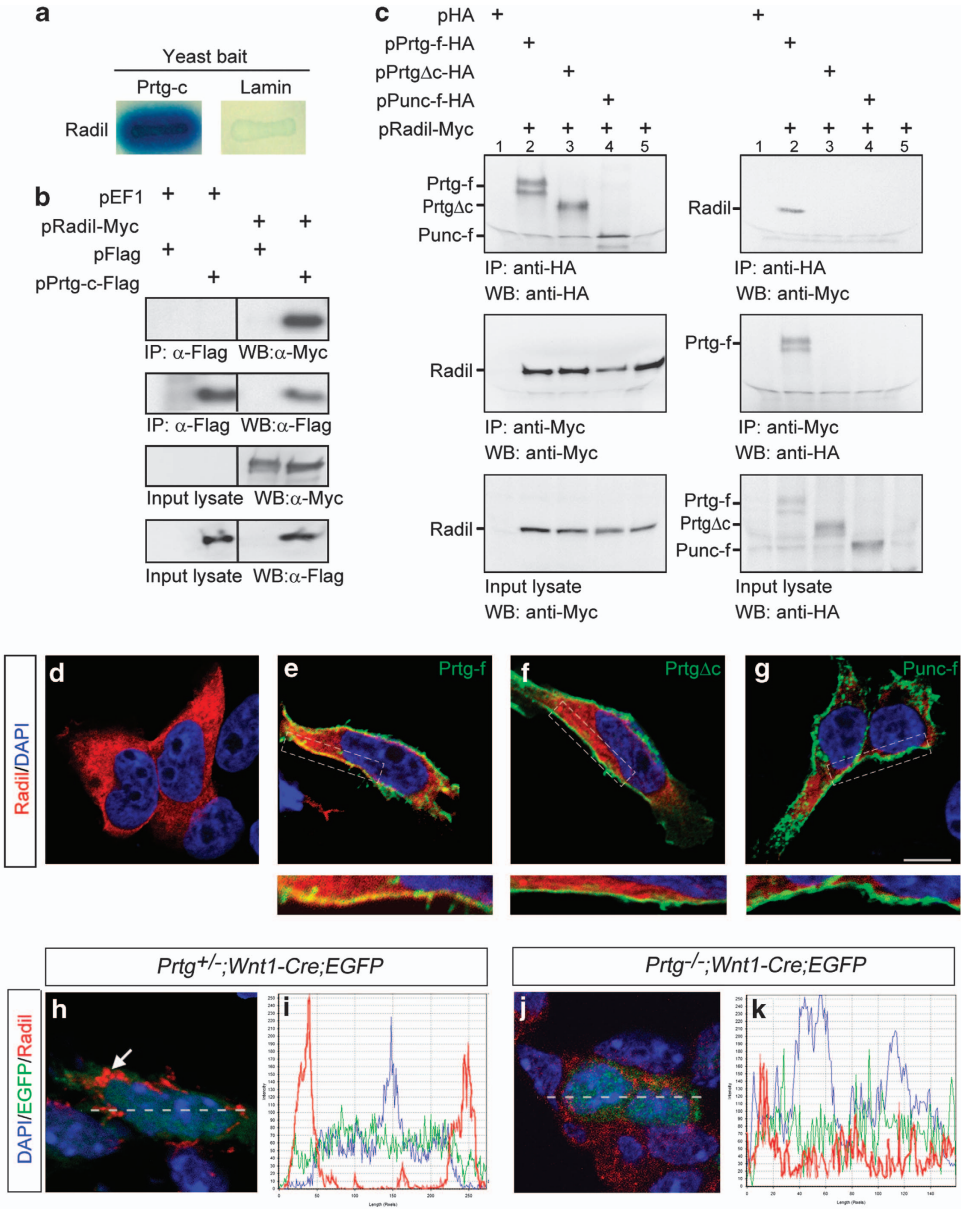

Figure 5 Prtg interacts with Radil. (**a**) Interaction between Radil and the cytoplsmic domain of Prtg (Prtg-c) or lamin is displayed as β-galactosidase activity in the yeast two-hybrid assay. (**b**) HEK293T cells were transfected with indicated plasmids. Cell lysates were immunoprecipitated with rabbit anti-Flag antibodies and subjected to western blot analysis with an anti-Myc or anti-Flag monoclonal antibody. (**c**) HEK293T cells were transfected with various plasmids. Cell lysates were immunoprecipitated with rabbit anti-HA antibodies (top panels) or rabbit anti-Myc antibodies (middle panels) and subjected to western blot analysis with the anti-Myc or anti-HA monoclonal antibody. (**d**–**g**) Myc-tagged Radil was cotransfected with indicated plasmids (all HA-tagged) into HEK293T cells. The subcellular localizations of the overexpressed proteins were labeled with mouse anti-Myc antibody or rabbit anti-HA antiserum and visualized using a confocal microscope. Images shown are representatives of 20 cells analyzed in at least three independent experiments. Lower panels are higher magnifications of the white boxes. Scale bar, 20 μm. (**h**, **j**) Confocal images of Radil (red) expressed in E9.0 R-CNCCs (green) from *Prtg*$^{+/-}$;*Wnt1-Cre;CAT-EGFPflox* and *Prtg*$^{-/-}$; *Wnt1-Cre;CAT-EGFPflox* embryos. Nuclei are labeled with DAPI (blue). (**i**, **k**) Relative fluorescence intensity plots of Radil, DAPI and EGFP along the dotted line shown in (**h**) and (**j**)

Mesp1-Cre;CAT-EGFP^{flox} or *Prtg*$^{-/-}$;*Mesp1-Cre;CAT-EGFP*^{flox} embryos. Furthermore, the earliest time point that defective alkaline phosphatase activity, an early marker of osteogenesis,[23] can be detected in parietal bone is at E15.5 (data not shown). As the defect occurs long after *Prtg* ceases to be expressed at E10, we reason that it is a consequential effect due to the loss of R-CNCCs.

Prtg protein interacts with Radil. We used the Prtg cytoplasmic domain (Prtg-c) as a bait to search molecules that mediate signaling of Prtg protein in a yeast two-hybrid assay. Among 1.5×10^6 independent clones, 58 DNA fragments were found to interact with Prtg-c. One of these, Radil, shows the strongest interaction with Prtg-c (Figure 5a). As the knockdown of Radil, a Rap1 GTPase interactor,

interrupts migration of NCCs and results in their apoptosis in zebrafish,[24] we thus focused on Radil as a putative Prtg downstream binding partner. Immunoprecipitation was performed using HEK293T cell lysates containing overexpressed Flag-tagged Prtg-c and Myc-tagged Radil. The anti-Flag immune complex was then subjected to western blotting. Radil is co-precipitated with Prtg-c (Figure 5b). Moreover, Radil interacts with Prtg-f but not with full-length Punc (Punc-f) (Figure 5c). The extracellular domain of Punc has the highest identity (43.8%) with that of Prtg.[25] The interaction between Prtg and Radil is mediated through the cytoplasmic domain of Prtg, as cytosolic domain-deleted Prtg (PrtgΔc) cannot associate with Radil (Figure 5c, lane 3).

We also analyzed interaction between Prtg and Radil at the cellular level. When overexpressed alone, Radil is localized in a cytoplasmic pool in HEK293T cells (Figure 5d and Ahmed *et al.*[26]). Overexpression of Prtg-f, but not PrtgΔc nor Punc-f, leads to the translocation of Radil to the plasma membrane where it colocalizes with Prtg-f (Figures 5e–g). In addition, when sections of E9.0 *Prtg*$^{+/-}$;*Wnt1-Cre*;*CAT-EGFPflox* embryos are examined with antibody against Radil, Radil is clustered as punctate particles concentrated along cell–cell junctions in R-CNCCs (Figures 5h and i); however, Radil is somewhat evenly distributed in Prtg-null R-CNCCs (Figures 5j and k), further supporting that Radil is recruited to plasma membrane by Prtg.

ERdj3/Prtg/Radil signaling promotes cell migration by inducing cell surface expression of the high-affinity $\alpha5\beta1$-integrin. As Radil was shown to control migration of NCCs in zebrafish,[24] we examined whether Prtg facilitates cell migration by recruiting Radil in the transwell migration assay using cultured AD293 cells. Ectopic expression of Radil or Prtg promotes $39 \pm 5\%$ and $45 \pm 7\%$ more cell migration, respectively (Figure 6a, bars 2 and 3). Overexpression of Radil and Prtg together in AD293 cells produces a synergistic effect that results in $107 \pm 13\%$ increase in cell migration (Figure 6a, bar 4). When conditioned medium (CM) containing ERdj3 (ERdj3-CM) is added to the lower chamber of the transwell, $309 \pm 69\%$ more cell migration is detected in AD293 cells overexpressing both Prtg and Radil (Figure 6a, bar 10). Effects of ERdj3 and Prtg on AD293 cell motility are completely abolished when Radil is knocked down by RNA interference (Figure 6b, bar 6 *versus* bar 8).

A recent study shows that Radil regulates adhesion of cultured cells on fibronectin by activating $\beta1$-integrin.[26] Furthermore, knockout of $\alpha5$-integrin triggers apoptosis of CNCCs.[13] We thus utilized cell cytometry to examine whether increased expression of high-affinity $\beta1$- and $\alpha5$-integrin subunits on the cell surface is the underlying mechanism responsible for cell mobility induced by ERdj3/Prtg/Radil signaling. Overexpression of either Prtg or Radil increases presentation of high-affinity $\beta1$- and $\alpha5$-integrin subunits on the plasma membrane (Figures 6c–f). An addition of ERdj3-CM to AD293 cells overexpressing both Prtg and Radil increases cell surface expression of high-affinity $\beta1$-integrin and $\alpha5$-integrin to about three times of the control level (Figures 6d and f, bar 8 *versus* bar 1). Note that the extent of increased expression of the activated $\beta1$- and $\alpha5$-integrin subunits induced by various treatments of ERdj3, Prtg and Radil match well to the levels of cell motility induced by these treatments. We further demonstrated that overexpressed Prtg is able to co-precipitate endogenous $\beta1$-integrin in AD293 cells in an immunoprecipitation assay (Figure 6g).

Expression of the high-affinity $\alpha5\beta1$-integrin decreases in Prtg-null R-CNCCs. We further interrogate levels of high-affinity $\alpha5\beta1$-integrins on R-CNCC cell membrane in *Prtg*$^{-/-}$;*Wnt1-Cre*;*CAT-EGFPflox* mutant embryos by immunofluorescence staining. About 35% less of immunofluorescence intensity of the activated $\beta1$-integrin subunit are detected in E9.0 Prtg-null R-CNCCs and rostral non-CNCCs; however, no change of the activated $\beta1$-integrin subunit expression is detected in Prtg-deficient TNCCs and non-TNCCs (Figures 7a–h, q). Expression of the activated $\alpha5$-integrin subunit in E9.0 R-CNCCs, but not rostral non-CNCCs, also decreases 20% in the absence of Prtg protein (Figures 7i–p and q). Note that amounts of total $\beta1$- and $\alpha5$-integrin subunits do not change in *Prtg*$^{-/-}$ mutant embryos (Figure 7r). To confirm there are fewer high-affinity $\alpha5\beta1$-integrins in Prtg-null R-CNCCs, we examined their cell mobility using the *in vitro* transwell assay. When dissociated cells isolated from E9.0 embryos were put to test, there were 45% fewer Prtg-null R-CNCCs migrating through the membrane than Prtg heterozygous R-CNCCs. In contrast, only 22% fewer Prtg-null rostral non-CNCCs migrate through the membrane than the Prtg heterozygous rostral non-CNCCs (Figure 7s). No difference in migration ability is detected in Prtg-null TNCCs and non-TNCCs. These results suggest that decreased expression of both high-affinity $\alpha5$- and $\beta1$-integrin subunits might exacerbate the deficiency of integrin activity in Prtg-null R-CNCCs.

Figure 6 ERdj3/Prtg/Radil signaling activates $\beta1$- and $\alpha5$-integrin in AD293 cells. (**a**, **b**) Quantitative results of the transwell assay. At 48 h after transfection, AD293 cells transfected with indicated plasmids were placed in the upper chamber. The lower chamber contained control CM or ERdj3-containing CM (ERdj3-CM). All data are normalized to the control vector (pEF1) and shown as the mean ± S.E.M. Statistic analysis are made between all samples and the control vector, and between samples connected by lines ($n = 3$; $^*P < 0.05$, by Student's *t*-test). (**c**, **e**) AD293 cells were transfected with indicated plasmids. At 16 h after transfection, cells were incubated with CM or ERdj3-CM for another 24 h before flow cytometry analyses of activated $\beta1$-integrin (**c**) or activated $\alpha5$-integrin (**e**). The gray area and the white area represent fluorescence distribution of cells treated with a control plasmid (pEF1) and indicated plasmids, respectively. The Mn^{2+}-treated group is used as a full activation control. (**d**, **f**) are quantitative data of (**c**) and (**e**). All data are normalized to the Mn^{2+}-treated control and shown as the mean ± S.E.M. ($n = 3$; $^*P < 0.05$, by Student's *t*-test). (**g**) Co-precipitation of activated β1-integrin with Prtg. Cell lysates of AD293 cells transfected with indicated plasmids (all Myc-tag) and cultured with/without ERdj3 were immunoprecipitated with anti-Myc antibody. The immunoprecipitates were subjected to western analysis with indicated antibodies. Lower four panels are immunoblots loaded with 20% of cell lysates used in immunoprecipitation

Discussion

NCCs are a transient population of cells that undergo epithelial-to-mesenchymal transition along the antero-posterior body axis. Depending on their origins in the neural tube, NCCs migrate and populate in cranial, cardiac, trunk and enteric domains.[3] In each domain, these cells enter into various tissues and become cell types that match the needs of that particular tissue by interacting with neighboring cells

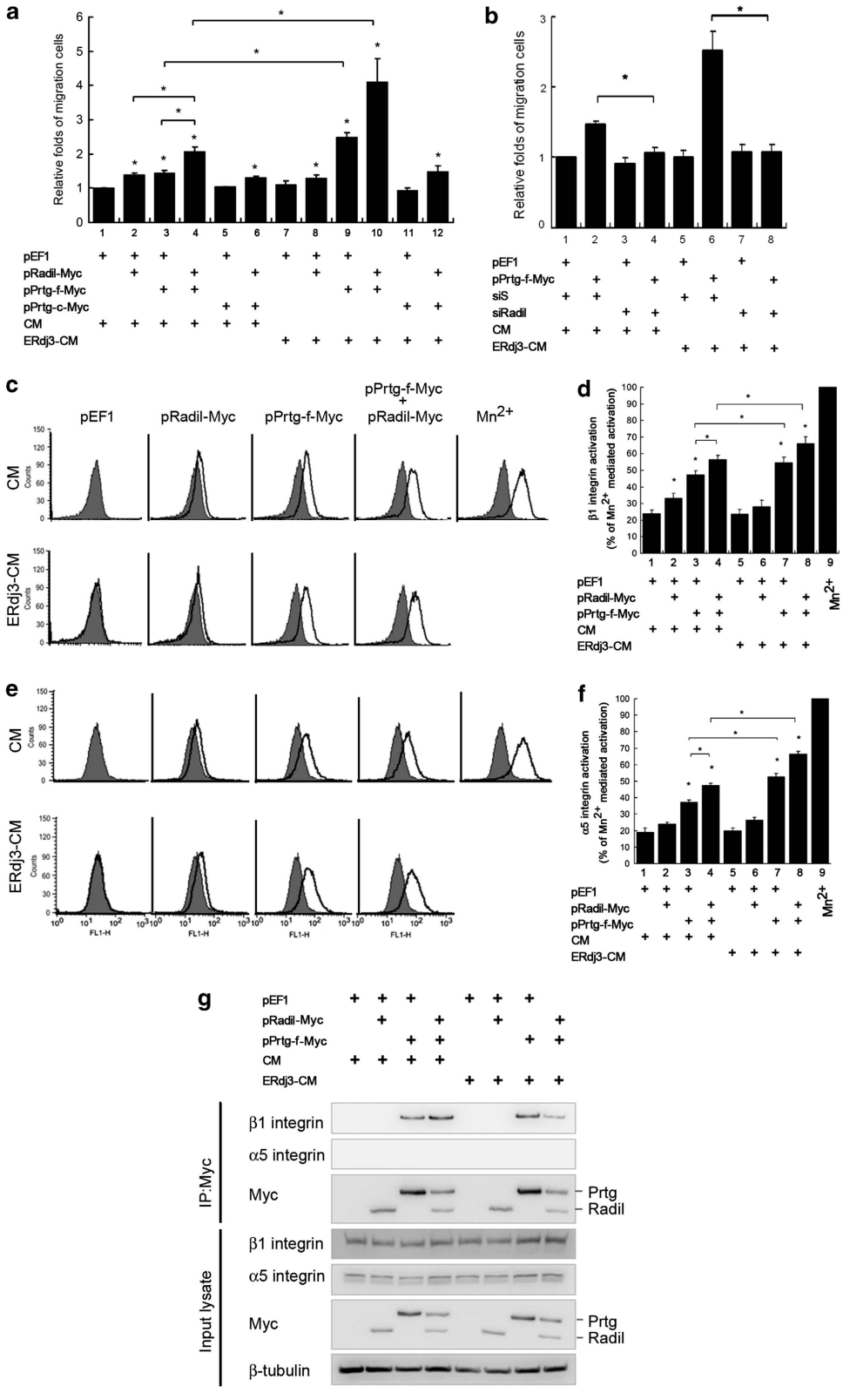

reciprocally. Here we report that an immunoglobulin family member, Prtg, is involved in the survival of R-CNCCs that contribute to the osteogenic and chondrogenic cells in the craniofacial structures. In *Prtg*$^{-/-}$ embryos, increased cell death is detected in R-CNCCs during E9–E10 (Figure 8a). Later in development, the loss of these cells delays the development of mesoderm-derived mesenchymal cells. These direct and indirect effects manifest the craniofacial phenotypes that we detect in *Prtg*$^{-/-}$ mutant mice at birth. We further provide *in vitro* evidence that Prtg recruits Radil to

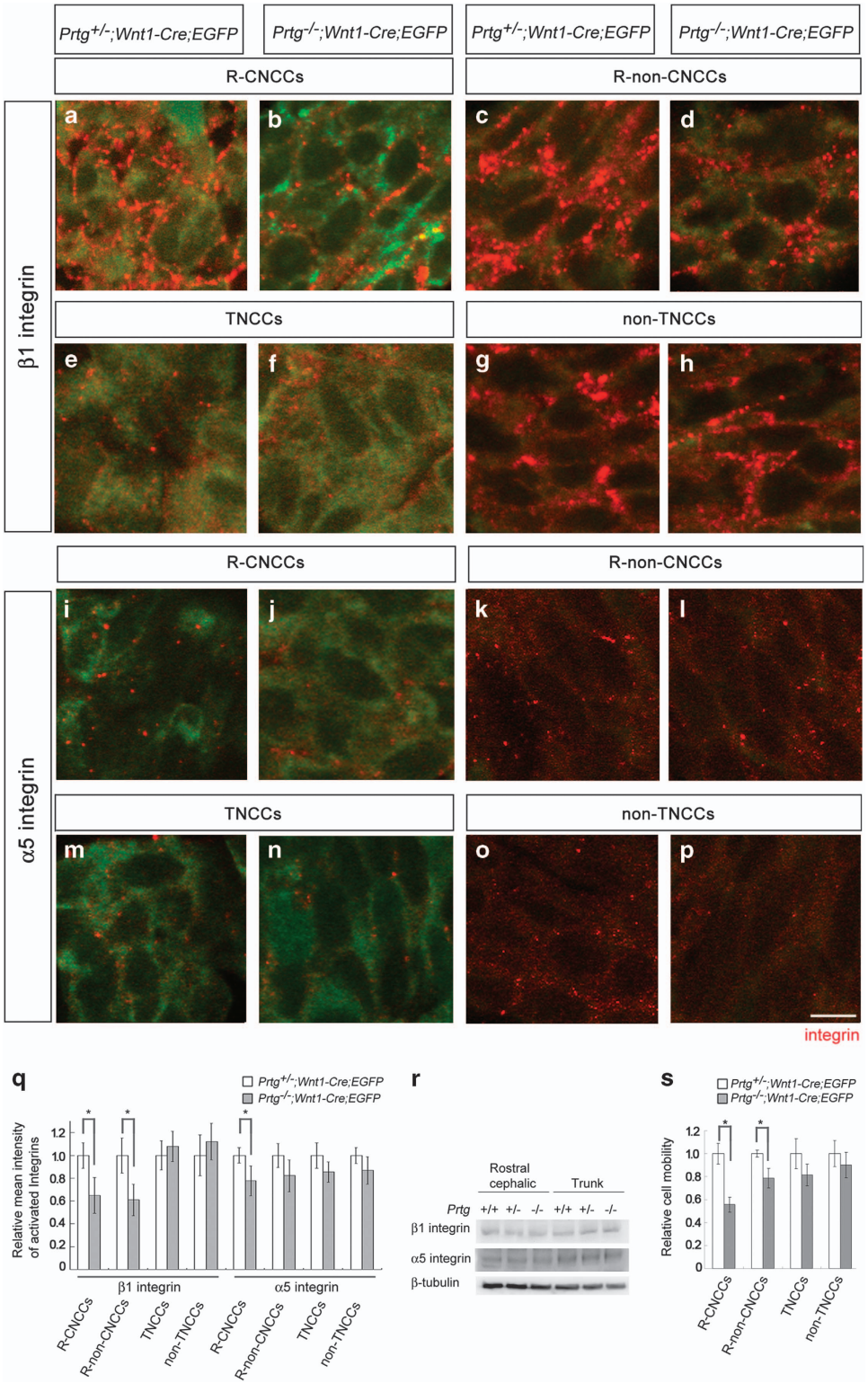

the plasma membrane, and subsequently changes the structure of the $\alpha5\beta1$-integrin to high-affinity conformation, and facilitates cell migration (Figure 8b). In the absence of Prtg proteins, fewer Radil proteins are translocated to the membrane, and consequently fewer $\alpha5\beta1$-integrins are activated to high-affinity conformation in *Prtg*$^{-/-}$ embryos; thus, a subset of R-CNCCs undergoes premature apoptosis. As Radil associates with Rap1, and talin is the converging point in the inside-out integrin activation,[26–28] ERdj3/Prtg/Radil signaling pathway may also involve Rap1 and talin to activate $\alpha5\beta1$-integrin (Figure 8b).

Signaling involved in the survival of R-CNCCs. Two possible, but not exclusive, scenarios may explain how cell death program is initiated in a subset of Prtg-deficient R-CNCCs as observed in this study. First, it had been shown that the $\alpha5\beta1$-integrin supports survival of cultured cells grown on fibronectin by upregulating Bcl-2 expression.[29] Signaling molecules, including Shc, FAK, Ras, PI3K and Akt, are required for the increase of *bcl-2* transcription induced by $\alpha5\beta1$-integrin activity.[30] It is thus likely that extracellular matrix molecules in *Prtg*$^{-/-}$ embryos cannot transmit survival signals for *Prtg*-deficient R-CNCCs due to insufficient amounts of the high-affinity $\alpha5\beta1$-integrin on plasma membrane of these cells. Alternatively, the migration defect may be the cause for R-CNCC death. In the absence of Prtg, insufficient exhibition of high-affinity $\alpha5\beta1$-integrin interrupts migration of a subset of R-CNCCs along their migratory pathways toward frontonasal primordium and BA1, thus preventing their access to the local survival factors, such as BMP2, BMP4 and FGF8.[22,31] Results that 45% fewer Prtg-null R-CNCCs migrate through the transwell membrane (Figure 7s) lend some support to the latter possibility. In addition, Smolen *et al.*[24] showed that the blockage of apoptosis is not able to prevent craniofacial defects observed in zebrafish after knocking down Radil, suggesting that effects of Radil are primarily on migration. Owing to many cells migrating at the same time in mouse E8.5–E9.0

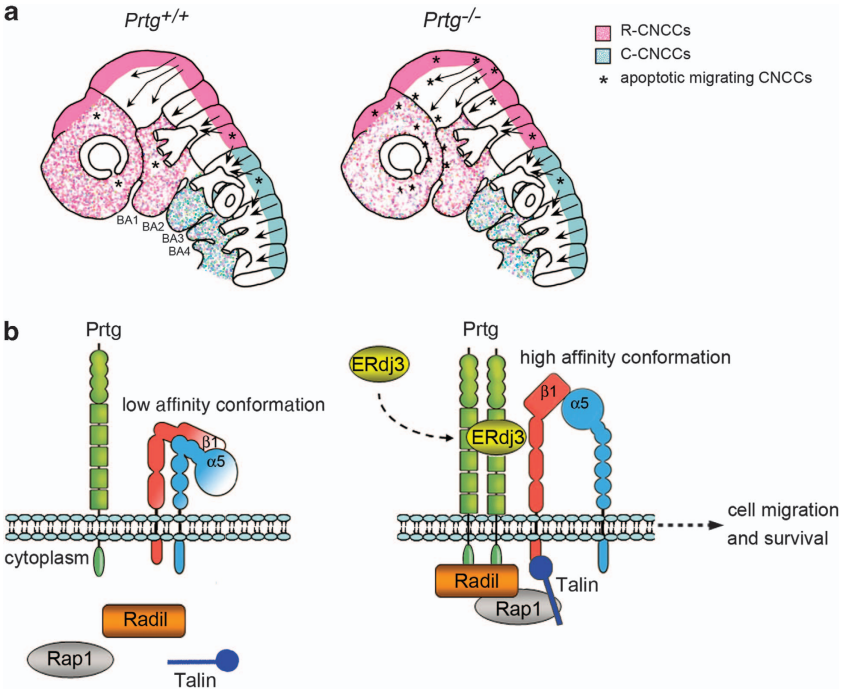

Figure 8 A proposed model of ERdj3/Prtg signaling for craniofacial bone formation. (**a**) R-CNCCs populate at fontonasal primodium and BA1 during E9–E10 (pink dots). Upon loss of Prtg, increased apoptosis of a subset of R-CNCCs (marked as *) occurs. (**b**) Stimulation of Prtg by ERdj3 in R-CNCCs recruits Radil, Rap1 and talin to form a complex, which induces conformational changes of the $\alpha5\beta1$-integrin. If expression of the high-affinity $\alpha5\beta1$-integrin reaches above a threshold, full migratory and survival signaling for R-CNCCs ensues

Figure 7 Lower levels of the activated $\alpha5\beta1$-integrin are expressed in the *Prtg*-null R-CNCCs. Transverse sections of *Prtg*$^{+/-}$;*Wnt1-Cre;CAT-EGFPflox* and *Prtg*$^{-/-}$;*Wnt1-Cre;CAT-EGFPflox* were labeled with the antibody against activated $\beta1$- (**a**–**h**) or activated $\beta5$-integrin (**i**–**p**). At the cephalic level (**a**–**d**), expression of the activated $\beta1$-integrin in *Prtg*$^{-/-}$ embryos is decreased in R-CNCCs and rostral non-CNCCs (R-non-CNCCs) (**b**, **d**) than in those in *Prtg*$^{+/-}$ embryos (**a**, **c**). No difference between *Prtg*$^{+/-}$ and *Prtg*$^{-/-}$ embryos is observed in TNCCs and trunk non-NCCs (**e**–**h**). Expression of the activated $\alpha5$-integrin is decreased in *Prtg*$^{-/-}$ R-CNCCs (**j**), but not in R-non-CNCCs, TNCCs and non-TNCCs (**l**, **n**, **p**). Scale bar, 10 μm. (**q**) Quantification of the mean fluorescence intensities of the activated $\beta1$- and $\alpha5$-integrin subunits in each cell in *Prtg*$^{+/-}$;*Wnt1-Cre;CAT-EGFPflox* and *Prtg*$^{-/-}$;*Wnt1-Cre;CAT-EGFPflox* embryos. Fluorescence intensities of more than 400 cells of each group were measured, and mean intensity was then calculated. Data (mean ± S.E.M.) were then normalized against those of *Prtg*$^{+/-}$ embryos ($n=4$; * $P<0.05$, by Student's *t*-test). (**r**) Expression of $\beta1$- and $\alpha5$–integrin subunits in embryos was analyzed by western blots. (**s**) Quantitative results of the cell mobility assay. Cells from different regions of *Prtg*$^{+/-}$;*Wnt1-Cre;CAT-EGFPflox* or *Prtg*$^{-/-}$;*Wnt1-Cre;CAT-EGFPflox* embryos were dissociated and subjected to transwell migration assay. Ratios of cells migrating through membrane were calculated and further normalized to the *Prtg*$^{+/-}$ groups and were shown as the mean ± S.E.M. ($n=3$; *$P<0.05$, by Student's *t*-test)

embryos and only a part of R-CNCCs is affected by *Prtg* deficiency, we were not able to resolve these two possibilities in this study. Finding a new way to label only a few R-CNCCs in mouse embryos and performing direct comparison of migration rates of R-CNCCs in control and $Prtg^{-/-}$ embryos will be needed to solve the issue.

Presence of a redundant gene(s) that substitutes loss of *Prtg*. Expression of Prtg protein in mesoderm begins as early as E7 and is present in almost all cells between E8.25 and E9.5, except in the notochord and differentiating cardiac cells.[15] When levels of *Prtg* mRNA are perturbed by an RNA interference approach in stage 6 chick embryos, ingression of paraxial mesoderm precursor cells is impaired.[17] If levels of *Prtg* mRNA are perturbed at stage 9, precocious neuronal differentiation in the developing chick neural tube occurs.[15] Furthermore, using a mouse mandible organ culture, Takahashi *et al.*[16] showed that knockdown of *Prtg* mRNA in tooth germ causes an arrest of the tooth development. These results suggest that Prtg may have roles in migration of primitive mesoderm cells, neuronal differentiation and tooth germ formation. Thus, it is unexpected that no embryonic lethality, no abnormality in the nervous system and no defects in dental tissue could be detected in $Prtg^{-/-}$ mutants. Further studies are required to find out why the discrepancy occurs and to search for the redundant gene compensating the loss of *Prtg* during development.

Materials and Methods

Animals. Adult C57BL/6J mice were obtained from the National Laboratory Animal Center (Taipei, Taiwan, ROC). *CAT-EGFPflox* mice were described previously.[32] *R26R* transgenic mice were kindly provided by Ting-Fen Tsai. *Wnt1-Cre* mice were purchased from the Jackson Laboratories (Bar Harbor, ME, USA). *Mesp1-Cre* mice were obtained from RIKEN BioResource Center (Ibaraki, Japan).[33] All mice were handled according to the university guidelines and experiments were approved by the National Yang-Ming University Animal Care and Use Committee. For the timed pregnancies, mice were set up in the late afternoon and when plugs were detected the next morning, this was designated as E0.5.

Materials. Expand high-fidelity *Taq* DNA polymerase, deoxynucleotides, 4′,6′-diamidino-2-phenylindole (DAPI), the *in situ* Cell Death Detection kit (TUNEL), reagents used in the *in situ* hybridization were obtained from Roche (Indianapolis, IN, USA). *Taq* DNA polymerase were purchased from Promega (Madison, WI, USA). The primers used in the PCRs were synthesized by MDBiol (Taipei, Taiwan). All other chemicals, unless otherwise specified, were purchased from Sigma (St. Louis, MO, USA).

Vector construction. The various *Prtg* plasmids had been constructed previously.[15] The mouse open reading frames of *Punc* and *Radil* were amplified by PCR using primers listed in Supplementary Table S1 and cloned to pEF1/Myc-His. The plasmids containing *Dlx5*, *Fgf8*, *Lhx7* and *Msx2* for *in situ* hybridization were provided by J Rubenstein (Department of Psychiatry, UCSF, San Francisco, CA, USA), Y-T Yan (Institute of Biomedical Sciences, Academia Sinica, Taipei, Taiwan), V Pachnis (National Institute for Medical Research, Medical Research Council, London, UK) and Y-H Liu (Department of Biochemistry and Molecular Biology, Kenneth R. Norris Cancer Hospital and Institute, Los Angeles, CA, USA), respectively. Other probes were generated by PCR using E9.5 mouse cDNA as template and cloned in pCRII-TOPO (Invitrogen, Grand Island, NY, USA). DNA fragments containing Radil sequences and scramble sequences (Supplementary Table S1) were cloned into pUI4-puro-SIBR to give rise to siRadil and siS. All plasmids were verified by restriction enzyme mapping and/or sequencing.

Antibodies. Mouse anti-Prtg monoclonal antibody (PRTG2, 1 μg/ml) has been described previously.[15] Mouse anti-β-tubulin antibody (E7, 1 : 10 000), mouse anti-neurofilament antibody (2H3, 1 : 900) and anti-Myc antibody (9E10, 1 : 5000) were obtained from the Developmental Studies Hybridoma Bank (University of Iowa, Iowa City, IA, USA). Rabbit monoclonal antibody against cCasp3 (5A1E, 1 : 400) was purchased from Cell Signaling (Danvers, MA, USA). Mouse anti-Flag M2 monoclonal antibody (1 : 1000) and rabbit anti-Flag polyclonal antiserum (1 : 1000) were purchased from Sigma. Mouse anti-activated α5-integrin antibody (SNAKA51, 10 μg/ml) was from Dr. MJ Humphries. Rabbit anti-α5-integrin antibody (1 : 1000) was from Chemicon (Billerica, MA, USA). Rat anti-β1-integrin antibody (9EG7, 10 μg/ml) was from BD Bioscience (San Jose, CA, USA). Rabbit anti-β1-integrin antibody (ab52971, 1 : 1000) was from Abcam (Cambridge, MA, USA). Rabbit anti-Radil antibody (1 : 300) was from Abgent (San Diego, CA, USA).

Targeted disruption of the mouse *Prtg* gene. The targeting vector was linearlized and electroporated into 129/Sv ES cells. G418-resistant ES colonies obtained by homologous recombination were selected by Southern blot hybridization. Two correctly targeted ES cell lines and one *Neo* pop-out ES cell line were injected into blastocysts and the resultant chimeras bred with C57BL/6J mice. Genotyping was performed by Southern blotting and/or PCR using the primers listed in Supplementary Table S1. Heterozygous F1 mice were backcrossed with C57BL/6J mice and mice after congenic N12 were used in the study.

Histological analysis, X-gal staining and whole-mount *in situ* hybridization. Embryos were dissected and fixed with 4% paraformaldehyde at 4 °C for 20 min (for X-gal staining), or overnight (for *in situ* hybridization and histological staining). For tissue sections, embryos were further soaked in 30% sucrose for overnight and then cryostat sectioned at 12 μm. For the histology, frozen sections were stained with hematoxylin–eosin using standard procedures. For whole-mount X-gal staining, the embryo were processed for β-galactosidase activity as described.[34] The *in situ* hybridization procedure was performed as described previously.[35] The protocols of staining with Alizarin red to reveal bone and Alcian blue to reveal cartilage were published previously.[36]

Detection of cell death. Transverse sections of embryos were cut at 12 μm and subjected to TUNEL assay and DAPI staining. Alternatively, sections were labeled with antibodies against cCasp3. The numbers of $TUNEL^+$ and $cCasp3^+$ cells were counted manually.

Yeast two-hybrid analysis. The rat Prtg-c (amino acids 966–1193) was cloned into the vector pBTM-116 as a bait. An E7 mouse embryo cDNA library fused to the GAL4 activation domain (Clontech) was used as the prey library. Other procedures have been described previously.[15]

Cell culture, protein extraction, immunoprecipitation and Western blotting. Previously described procedures were followed for these experiments.[15]

Migration assay. Human AD293 cells were transfected with different plasmids using calcium phosphate method and cultured for 2 days in 10% FBS/DMEM at 37 °C in a 5% CO_2 incubator. Cells were then detached from culture dishes using 1 μM EDTA and resuspended in 0.5% FBS/DMEM medium. A total of 1×10^5 cells was seeded to the migration chamber (Millicell with 8 μm pore size; Millipore, Billerica, MA, USA); the lower chambers contained CM collected from pEF1- or pERdj3-transfected HEK293T cells that were cultured in 0.5% FBS/DMEM from 24 to 72 h after transfection. Duration of migration lasted 4 h and migratory cells were stained with Hoechst 33258 and quantified by counting four random fields.

For detection of primary cell mobility, tissues from rostral cephalic region and trunk region were dissected from E9.0 (15–18 somite stage) embryos and dissociated with collagenase (0.75 mg/ml) at 37°C for 5 min.[37] Dissociated cells were filtered through 40 μm cell strainers (BD Falcon, San Jose, CA, USA). A total of 3×10^3 cells were seeded to the upper chamber coated with fibronectin. Duration of migration lasted 5 h. $EGFP^+$ and $EGFP^-$ cells in the upper chambers and bottom chambers were fixed and stained with DAPI, and quantified under a fluorescence microscope. The ratio of migration is defined as cell numbers of the bottom chambers divided by the total cell numbers in both chambers and normalized to that of control embryos.

Flow cytometry. AD293 cells were dissociated with trypsin, washed two times with PBS, re-suspended in DMEM containing 0.1% BSA and 20 mM HEPES, pH 7.4. Cells were then recovered at room temperature for 30 min. Cells were incubated with anti-β1-integrin (9EG7) or anti-α5-integrin (SNAKA51) antibody at room temperature for 1 h. For positive control, 2 mM Mn^{2+} was added when cells were incubated with primary antibodies. Cells were washed three times with PBS and incubated with Alexa-488-conjugated donkey anti-rat IgG or Alexa-488-conjugated donkey anti-mouse IgG (Jackson ImmunoResearch, Baltimore, PA, USA) at room temperature for 45 min. After three washes in PBS, cells were fixed in 4% paraformaldehyde at room temperature for 15 min and re-suspended in PBS. Flow cytometry measurement was taken in a FACSCalibur flow cytometer using the CellQuest Pro software (BD Biosciences) for data acquisition and analysis. Integrin activation was expressed as the ratio of the mean of fluorescence to the Mn^{2+}-treated group.

Conflict of Interest

The authors declare no conflict of interest.

Acknowledgements. We thank LS Kao, L-J Lo, T-W Wang and J-Y Yu for discussion and critical reading of the manuscript, MC Colbert for providing *CAT-EGFPflox* mice, MJ Humphries for SNAKA51 and the Developmental Studies Hybridoma Bank for providing monoclonal antibodies. This research was supported by National Science Council (NSC95-2320-B-010-059-MY2 and NSC99-2321-B-010-016) and the Ministry of Education (Aim for the Top University Plan) to M-J Fann.

Author contributions

Y-CW, H-CJ, Y-HW and M-JF conceived and designed the experiments. Y-CW, H-CJ, Y-HW, W-CK, Y-LL, S-FL and C-JL conducted experiments. Y-CW and M-JF wrote the manuscript.

1. Farlie PG, McKeown SJ, Newgreen DF. The neural crest: basic biology and clinical relationships in the craniofacial and enteric nervous systems. *Birth Defects Res C* 2004; **72**: 173–189.
2. Trainor PA, Tan SS, Tam PP. Cranial paraxial mesoderm: regionalisation of cell fate and impact on craniofacial development in mouse embryos. *Development* 1994; **120**: 2397–2408.
3. Le Douarin NM, Kalcheim C. *The Neural Crest*. 2nd edn. Cambridge University Press: New York, NY, USA, 1999.
4. Minoux M, Rijli FM. Molecular mechanisms of cranial neural crest cell migration and patterning in craniofacial development. *Development* 2010; **137**: 2605–2621.
5. Etchevers HC, Vincent C, Le Douarin NM, Couly GF. The cephalic neural crest provides pericytes and smooth muscle cells to all blood vessels of the face and forebrain. *Development* 2001; **128**: 1059–1068.
6. Le Douarin NM, Creuzet S, Couly G, Dupin E. Neural crest cell plasticity and its limits. *Development* 2004; **131**: 4637–4650.
7. Dupin E, Calloni GW, Le Douarin NM. The cephalic neural crest of amniote vertebrates is composed of a large majority of precursors endowed with neural, melanocytic, chondrogenic and osteogenic potentialities. *Cell Cycle* 2010; **9**: 238–249.
8. Trainor PA, Tam PP. Cranial paraxial mesoderm and neural crest cells of the mouse embryo: co-distribution in the craniofacial mesenchyme but distinct segregation in branchial arches. *Development* 1995; **121**: 2569–2582.
9. Bronner-Fraser M. An antibody to a receptor for fibronectin and laminin perturbs cranial neural crest development *in vivo*. *Dev Biol* 1986; **117**: 528–536.
10. Bronner-Fraser M. Alterations in neural crest migration by a monoclonal antibody that affects cell adhesion. *J Cell Biol* 1985; **101**: 610–617.
11. Testaz S, Delannet M, Duband J-L. Adhesion and migration of avian neural crest cells on fibronectin require the cooperating activities of multiple integrins of the β1 and β3 families. *J Cell Sci* 1999; **112**: 4715–4728.
12. Alfandari D, Cousin H, Gaultier A, Hoffstrom BG, DeSimone DW. Integrin $\alpha5\beta1$ supports the migration of *Xenopus* cranial neural crest on fibronectin. *Dev Biol* 2003; **260**: 449–464.
13. Goh KL, Yang JT, Hynes RO. Mesoderm defects and cranial neural crest apoptosis in α5 integrin-null embryos. *Development* 1997; **124**: 4309–4319.
14. Strachan LR, Condic ML. Neural crest motility on fibronectin is regulated by integrin activation. *Exp Cell Res* 2008; **314**: 441–452.
15. Wong Y-H, Lu A-C, Wang Y-C, Cheng H-C, Chang C, Chen P-H *et al*. Protogenin defines a transition stage during embryonic neurogenesis and prevents precocious neuronal differentiation. *J Neurosci* 2010; **30**: 4428–4439.
16. Takahashi KF, Kiyoshima T, Kobayashi I, Xie M, Yamaza H, Fujiwara H *et al*. Protogenin, a new member of the immunoglobulin superfamily, is implicated in the development of the mouse lower first molar. *BMC Dev Biol* 2010; **10**: 115.
17. Ito K, Nakamura H, Watanabe Y. Protogenin mediates cell adhesion for ingression and re-epithelialization of paraxial mesodermal cells. *Dev Biol* 2011; **351**: 13–24.
18. McBratney-Owen B, Iseki S, Bamforth SD, Olsen BR, Morriss-Kay GM. Development and tissue origins of the mammalian cranial base. *Dev Biol* 2008; **322**: 121–132.
19. Jiang X, Rowitch SH, Soriano P, McMahon AP, Sucov HM. Fate of the mammalian cardiac neural crest. *Development* 2000; **127**: 1607–1616.
20. Takahashi K, Nuckolls GH, Takahashi I, Nonaka K, Nagata M, Ikura T *et al*. Msx2 is a repressor of chondrogenic differentiation in migratory cranial neural crest cells. *Dev Dyn* 2001; **222**: 252–262.
21. Hunt P, Gulisano M, Cook M, Sham MH, Faiella A, Wilkinson D *et al*. A distinct Hox code for the branchial region of the vertebrate head. *Nature* 1991; **353**: 861–864.
22. Trumpp A, Depew MJ, Rubenstein JL, Bishop JM, Martin GR. Cre-mediated gene inactivation demonstrates that FGF8 is required for cell survival and patterning of the first branchial arch. *Genes Dev* 1999; **13**: 3136–3148.
23. Tsai MT, Li WJ, Tuan RS, Chang WH. Modulation of osteogenesis in human mesenchymal stem cells by specific pulsed electromagnetic field stimulation. *J Orthop Res* 2009; **27**: 1169–1174.
24. Smolen GA, Schott BJ, Stewart RA, Diederichs S, Muir B, Provencher HL *et al*. A Rap GTPase interactor, RADIL, mediates migration of neural crest precursors. *Genes Dev* 2007; **21**: 2131–2136.
25. Vesque C, Anselme I, Couve E, Charnay P, Schneider-Maunoury S. Cloning of vertebrate Protogenin (Prtg) and comparative expression analysis during axis elongation. *Dev Dyn* 2006; **235**: 2836–2844.
26. Ahmed SM, Daulat AM, Meunier A, Angers S. G protein $\beta\gamma$ subunits regulate cell adhesion through Rap1a and its effector Radil. *J Biol Chem* 2010; **285**: 6538–6551.
27. Han J, Lim CJ, Watanabe N, Soriani A, Ratnikov B, Calderwood DA *et al*. Reconstructiing and deconstructing agonist-induced activation of integin αIIbβ3. *Curr Biol* 2006; **16**: 1796–1806.
28. Tadokoro S, Shattil SJ, Eto K, Tai V, Liddington RC, de Pereda JM *et al*. Talin binding to integrin® tails: a final common step in integrin activation. *Science* 2003; **302**: 103–106.
29. Zhang Z, Vuori K, Reed JR, Ruoslahti E. The $\langle 5^{®}1$ integrin supports survival of cells on fibronectin and up-regulates Bcl-2 expression. *Proc Natl Acad Sci USA* 1995; **92**: 6161–6165.
30. Matter ML, Ruoslahti E. A signaling pathway from the $\alpha5\beta1$ and $\alpha v\beta3$ integrins that elevates bcl-2 transcription. *J Biol Chem* 2001; **276**: 27757–27763.
31. Barlow AJ, Francis-West PH. Ectopic application of recombinant BMP-2 and BMP-4 can change patterning of developing chick facial primordia. *Development* 1997; **124**: 391–398.
32. Nakamura T, Colbert MC, Robbins J. Neural crest cells retain multipotential characteristics in the developing valves and label the cardiac conduction system. *Circ Res* 2006; **98**: 1547–1554.
33. Saga Y, Miyagawa-Tomita S, Takagi A, Kitajima S, Miyazaki J, Inoue T. MesP1 is expressed in the heart precursor cells and required for the formation of a single heart tube. *Development* 1999; **126**: 3437–3447.
34. Hogan B, Beddington R, Costantini F, Lacy E. *Manipulating The Mouse Embryo: A Laboratory Manual*. 2nd edn Cold Spring Harbor Laboratory Press: Cold Spring Harbor, NY, USA, 1994.
35. Shen MM, Wang H, Leder P. A differential display strategy identifies Cryptic, a novel EGF-related gene expressed in the axial and lateral mesoderm during mouse gastrulation. *Development* 1997; **124**: 429–442.
36. Belo JA, Leyns L, Yamada G, De Robertis EM. The prechordal midline of the chondrocranium is defective in Goosecoid-1 mouse mutants. *Mech Dev* 1998; **72**: 15–25.
37. Shah NM, Marchionni MA, Isaacs I, Stroobant P, Anderson DJ. Glial growth factor restricts mammalian neural crest stem cells to a glial fate. *Cell* 1994; **77**: 349–360.

Supplementary Information accompanies this paper on Cell Death and Disease website (http://www.nature.com/cddis)